



Cite this: *Phys. Chem. Chem. Phys.*,
2020, 22, 18606

Free electron laser infrared action spectroscopy of nitrous oxide binding to platinum clusters, $\text{Pt}_n(\text{N}_2\text{O})^{+\dagger}$

Gabriele Meizyte,^{id a} Alice E. Green,^{id a} Alexander S. Gentleman,^{id a}
 Sascha Schaller,^{id b} Wieland Schöllkopf,^{id b} André Fielicke^{id *bc} and
 Stuart R Mackenzie^{id *a}

Infrared multiple-photon dissociation spectroscopy has been applied to study $\text{Pt}_n(\text{N}_2\text{O})^+$ ($n = 1-8$) clusters which represent entrance-channel complexes on the reactive potential energy surface for nitrous oxide decomposition on platinum. Comparison of spectra recorded in the spectral region 950 cm^{-1} to 2400 cm^{-1} with those simulated for energetically low-lying structures from density functional theory shows a clear preference for molecular binding *via* the terminal N atom, though evidence of O-binding is observed for some cluster sizes. Enhanced reactivity of Pt_n^+ $n \geq 6$ clusters towards N_2O is reflected in the calculated reactive potential energy surfaces and, uniquely in the size range studied, $\text{Pt}_6(\text{N}_2\text{O})^+$ proved impossible to form in significant number density even with cryogenic cooling of the cluster source. Infrared-driven N_2O decomposition, resulting in the formation of cluster oxides, Pt_nO^+ , is observed following vibrational excitation of several $\text{Pt}_n(\text{N}_2\text{O})^+$ complexes.

Received 23rd May 2020,
Accepted 27th July 2020

DOI: 10.1039/d0cp02800b

rsc.li/pccp

1. Introduction

Nitrous oxide (N_2O) is a significant atmospheric pollutant both as a greenhouse gas (GHG) and for the role it plays in ozone depletion.¹ As a result of its relatively high global warming potential (GWP) coefficient N_2O is considered to be the third principal long-lived GHG after CO_2 and CH_4 ,² and one of the most potent waste gases resulting from human activity that has a significant impact on both the future ozone layer and climate.³ N_2O discharge is not covered by the Montreal Protocol⁴ but, given its harmful environmental impact, there is considerable interest in using heterogeneous catalysis to reduce anthropogenic emissions.⁵

The platinum group metals (Ru, Rh, Pd, Os, Ir & Pt) are well-known heterogeneous catalysts. Platinum metal itself shows versatile catalytic abilities and is frequently used in industrial as well as everyday applications. For example, the production of nitric acid for fertilizers involves ammonia oxidation using a

platinum catalyst.⁶ However, platinum is probably best known for its role, along with palladium and rhodium, in promoting exhaust gas reactions in the automobile catalytic converter (design first developed by R. C. Stempel *et al.*⁷). Highly inert (noble even) in its bulk form, most catalytic applications of platinum make use of it in highly divided, often nanoscale form. In addition to maximizing surface area, this introduces defects into the metal which are not present in extended single crystal surfaces and it is these defect sites which often provide the sites for interesting chemistry.^{8,9}

Transition metal clusters serve as tractable model systems for the study of heterogeneous nanocatalysts at the molecular level.¹⁰ In the gas phase, the fundamental interactions involved in reactive chemistry can be studied in the absence of complex interactions present in real catalysts, such as the influence of substrates, solvation, and aggregation effects, which are challenging to analyse and often obscure the fundamental interactions of interest.¹¹ The subject of this study, isolated $\text{Pt}_n(\text{N}_2\text{O})^+$ clusters, represent model entrance-channel complexes for the initial chemisorption step in the metal-catalysed decomposition of N_2O .

Reflecting the catalytic properties of platinum, the reactions of platinum clusters, $\text{Pt}_n^{+/0/-}$, have received considerable attention previously. A variety of experimental techniques, including flow reactor, molecular beam-gas cell studies, and Fourier-transform ion-cyclotron resonance (FT-ICR) mass spectrometry, have been employed to study the reactions of $\text{Pt}_n^{+/0/-}$ with small

^a Department of Chemistry, University of Oxford, Physical and Theoretical Chemistry Laboratory, South Parks Road, Oxford, OX1 3QZ, UK. E-mail: stuart.mackenzie@chem.ox.ac.uk

^b Fritz-Haber-Institut der Max-Planck-Gesellschaft, Faradayweg 4-6, 14195 Berlin, Germany. E-mail: fielicke@fhi-berlin.mpg.de

^c Institut für Optik und Atomare Physik, Technische Universität Berlin, Hardenbergstraße 36, 10623 Berlin, Germany

[†] Electronic supplementary information (ESI) available: Containing calculated structures of important species observed experimentally, plus calculated N_2O binding energies and bond lengths. See DOI: 10.1039/d0cp02800b



molecules. These include dehydrogenation of small hydrocarbons,^{12–18} as well as H₂, CO₂, N₂O *etc.*^{19–23} Pt₄⁺ exhibits particularly low reactivity, also supported by a theoretical investigation,²⁴ and a photofragmentation study of bare Pt_n⁺ clusters by Janssens²⁵ suggests the reason lies in the anomalously large HOMO–LUMO gap for tetrahedral Pt₄⁺. Interestingly, Pt₄[–] activates carbon dioxide²⁶ and dehydrogenates methane very efficiently, perhaps because of its own planar structure.^{18,26}

Of particular relevance here are the single collision studies of Pt_n^{+/-} reactions with N₂O in which the cationic clusters exhibit dramatic size-dependent rate constants changing by several orders of magnitude upon the addition of a single metal atom.²² In this small cluster regime, every atom counts. In all cases the reaction proceeds exclusively *via* an O atom transfer generating sequential cluster oxides, Pt_nO_m⁺. Additional collisions are required to stabilize the molecular adsorption of N₂O.

Several studies have established catalytic abilities and even full cycles using platinum clusters. Water formation was observed in the catalytic oxidation of H₂ on Pt_n for $n = 7–30$ by Andersson and Rosén¹⁹ and Shi and Ervin²⁷ found small Pt_n[–] ($n = 3–6$) cluster anions to be effective catalysts for CO oxidation under thermal conditions. A full catalytic cycle of CO oxidation/N₂O reduction for Pt_n⁺ ($n = 6–8$) was reported by Beyer, Bondybey, and coworkers.²⁸

N₂O represents an interesting adsorbate for infrared studies, with the possibility of both N- or O-binding reflected in the degree of activation. This is very clearly observed in infrared action spectroscopy of N₂O binding at single metal centers, for example, M⁺(N₂O)_n (M = Cu, Ag, Au,²⁹ Co, Rh, Ir,³⁰ and Li, Al³¹) by Cunningham *et al.* These studies have revealed interesting binding motifs and structural isomers as well as the important role played by low-lying electronically excited states.

We have previously studied N₂O adsorption on small gas-phase Rh_n⁺ clusters (Rh_n(N₂O)⁺, $n = 4–8$)^{32,33} using the same methods to those employed in this work. Interesting IR-induced reactivity was observed in which excitation of infrared active modes results in N₂O decomposition and cluster oxide formation. Rh₅⁺ proved special in this regard with a single co-adsorbed oxygen atom changing the chemistry observed from N₂O loss on Rh₅(N₂O)⁺ to Rh₅O₂⁺ formation from Rh₅(ON₂O)⁺.³⁴ These results, along with those from related blackbody infrared³⁵ and collisional excitation studies³⁶ were explained in terms of relative reaction barriers and dissociation thresholds demonstrating how spectral characterization of entrance-channel complexes yields important information on the full reactive potential energy surface.

Here we report the first experimental investigation of cationic platinum clusters with adsorbed nitrous oxide, Pt_n(N₂O)⁺ ($n = 1–8$), using infrared multiple-photon dissociation spectroscopy. Cluster structures, along with relative cluster reactivities, are revealed with the help of complementary quantum chemical calculations.

II. Experimental methods

The infrared multiple-photon dissociation (IR-MPD) spectra presented in this report were recorded at the Fritz Haber Institute

(FHI) in Berlin making use of the FHI free electron laser (FEL)³⁷ facility. The experimental setup has been described in detail previously^{38,39} and only essential details are described here. Briefly, a rotating natural Pt target is ablated by a Nd:YAG laser (532 nm, 10 Hz). Ablated atoms cool and cluster by colliding with helium within a reaction channel, to which nitrous oxide is added by an additional late-mixing pulsed valve, downstream of the ablation point. The resulting gas mix, now entrained with a range of pure and decorated clusters, expands into the vacuum forming a molecular beam which is then skimmed before entering the extraction region of a reflectron time-of-flight (ToF) mass spectrometer used to detect the presence of cationic species. In an attempt to suppress direct oxidation and maximize the generation of molecularly bound Pt_n(N₂O)⁺ clusters, the cluster source was cooled with liquid nitrogen.

To record infrared multiple-photon dissociation (IR-MPD) spectra, the cluster beam is subjected to alternate pulses of output of the FHI FEL, operating for these purposes in the 950–2400 cm^{–1} range and corresponding parent ion depletion and fragment(s) channel enhancement are recorded as a function of wavenumber. In this way the spectra yield information on the infrared active modes of the parent cluster as well as dissociation branching ratios, which can be compared with the results of DFT simulations.

III. Computational methods

Energetically low-lying structures and relevant transition states connecting them have been calculated at the def2TZVP⁴⁰/TPSSH^{41,42} level, using the Gaussian 16 software package.⁴³ This functional reproduces the transition metal–ligand bond dissociation energies⁴⁴ and showed similar energetic ordering of the Pt_nO₂CO⁺ cluster geometries⁴⁵ to using the TPSS⁴² functional that has previously proved to generate reliable IR-MPD experimental results.^{46,47} The GD3-BJ dispersion term⁴⁸ was introduced to account for weak intramolecular interactions and a quasirelativistic Wood-Boring effective core potential (WB-ECP)⁴⁹ was used to freeze 60 inner electrons and introduce relativistic corrections for Pt atoms. As starting structures, the coordinates of bare Pt_n⁺ clusters for $n = 3–5$ were taken from earlier work by Harding *et al.*⁴⁷ To provide a better match with experimental data, computed harmonic vibrational frequencies were scaled by a factor of 0.955, determined by calculating the vibrational frequency of the asymmetric free N₂O band.⁵⁰ All energies reported here include zero point energies. Potential energy profiles were generated by identifying plausible transition states between two minima and performing Intrinsic Reaction Coordinate (IRC)^{51,52} calculations in order to verify the correct path.

IV. Results and discussion

A. Time-of-flight spectra and analysis

Fig. 1(a) shows part of the time-of-flight spectrum for the species produced following ablation of a natural platinum target in the presence of helium with low pressure nitrous oxide introduced downstream *via* the late mixing valve. We have repeated the



experiment at a range of N₂O pressures and these results are representative. A range of Pt_nO_x⁺ and Pt_n(N₂O)_m⁺ clusters are observed. We have previously reported an IR-MPD study of platinum oxide clusters.⁵³ Analysis of the time-of-flight spectrum is complicated by the fact that platinum has six stable isotopes, leading to a wide range of masses for the same chemical species. Nevertheless, deconvolution is possible and is illustrated in Fig. 1(b) for the Pt₃⁺X species produced. Pt_nO_x⁺ (x = 1, 2, 3) and Pt_n(N₂O)_m⁺ (m = 1, 2, 3) dominate the mass spectrum but a trace of Pt₃C⁺ and Pt₃CO⁺ is also observed – the carbon assumed to originate from polishing the target rod.

Quantitative analysis of the mass spectrum, including deconvolution for the isotopes of platinum, leads to the normalized product abundances shown in Fig. 2(a) which yield important information on the relative reactivity of different Pt_n⁺ cluster sizes towards N₂O. Reactivity pathways can be visualized as:

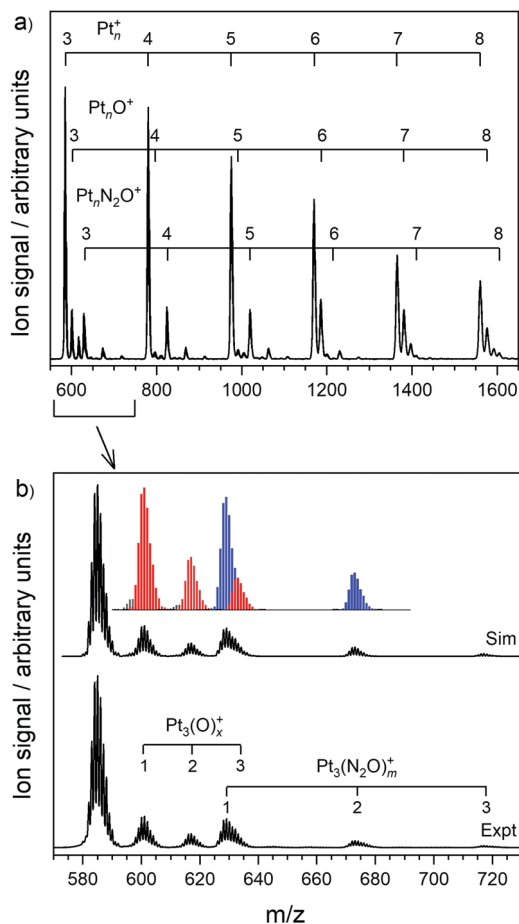
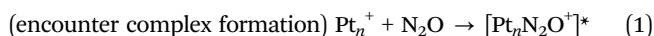


Fig. 1 (a) Time-of-flight mass spectrum; (b) (lower) experimental and (upper) simulated time-of-flight mass spectrum of Pt₃⁺ clusters – both produced by laser ablation of a natural platinum rod in helium to which nitrous oxide is added downstream. The cluster source was cooled to –140 °C with liquid N₂. The principal species produced are simple cluster oxides, Pt₃O_x⁺, and Pt₃(N₂O)_m⁺ with traces of Pt₃C⁺ and Pt₃CO⁺.

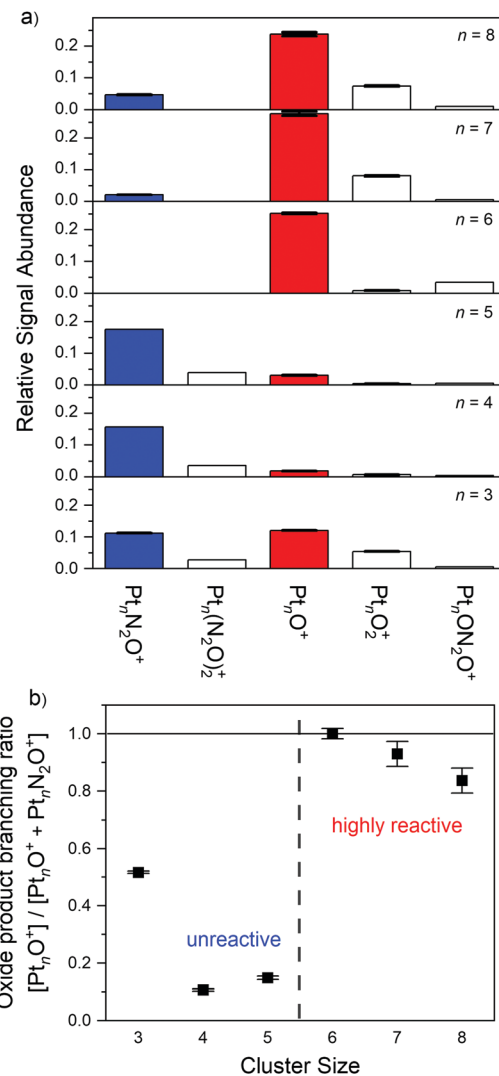
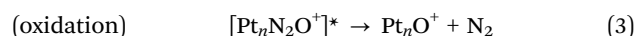
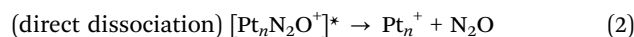
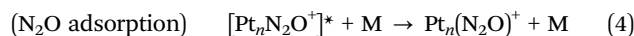


Fig. 2 (a) Histogram with normalised ion abundances (to a unity within each *n*; Pt_n⁺ not shown) for reaction products generated in the cluster source by the reaction of Pt_n⁺ (*n* = 3–8) with N₂O. The uncertainties shown reflect the fitting of overlapping isotope patterns for different species (see inset Fig. 1(b)); (b) fractional oxide production as a measure of Pt_n⁺ + N₂O reactivity. A step change in reactivity occurs between *n* = 5 and 6.

In the absence of additional collisions or radiative cooling, this complex must either dissociate or react, in all probability forming the simple cluster oxide for which evidence is observed in the mass spectrum:



The multiple-collision conditions of the cluster source reaction channel permit stabilisation of the initial complex, trapping it in an entrance-channel minimum of the reactive potential energy surface:



By measuring the charged products we are blind to process (2) but the relative branching ratios for the oxidation reaction



(3) and molecular adsorption (4) can be quantified as a function of cluster size.

For the $n = 3$ cluster under these approximately thermal, multiple collision conditions, the branching ratios for processes (3) and (4) are similar. For $n = 4, 5$ clusters, however, minimal cluster oxide formation is observed, with $\text{Pt}_n\text{N}_2\text{O}^+$ being the dominant product. For $n \geq 6$ the situation changes markedly and oxide production dominates. Indeed, for $n = 6$ itself, negligible $\text{Pt}_6\text{N}_2\text{O}^+$ is observed. This change in reactivity is highlighted in Fig. 2(b) which shows the Pt_nO^+ signal as a fraction of total primary products $[\text{Pt}_n\text{O}^+]/\{[\text{Pt}_n\text{O}^+] + [\text{Pt}_n\text{N}_2\text{O}^+]\}$ as a function of cluster size. The reactions reported here occur under very different conditions to the single collision experiments performed by Balteanu *et al.*²² in which only the direct oxidation process (3) was observed due to the lack of stabilizing collisions required for process (4). Nevertheless, the same step increase in reactivity between $n = 5$ and 6 is observed.

In an attempt to better understand the reactivity data, IRC profiles for cluster sizes $n = 4-6$ were calculated, as shown in Fig. 3. In each case, the two minima towards the left hand side represent O- and N-bound entrance-channel complexes of the respective $\text{Pt}_n(\text{N}_2\text{O})^+$ species and TS1 – a transition state for N_2O rotation connecting the two. These entrance channels are separated from the product channel by a potential barrier TS2, which involves significant N_2O rearrangement, ultimately leading to the production of Pt_nO^+ cluster and molecular nitrogen. In all cases the overall reaction is calculated to be exothermic by more than 1 eV.

The difference in reactivity between Pt_4^+ and Pt_6^+ (reported by Balteanu *et al.*²² as more than three orders of magnitude) is readily attributed to the fact that whilst the former has a real barrier on the ground state surface, in the latter the barrier is submerged. Calculations also show no reactive barrier for either of the two energetically low-lying electronic states of the $n = 5$ cluster and thus it is harder to explain the apparent lack of reactivity of this cluster. We note, however, that Balteanu *et al.* found Pt_5^+ to have intermediate reactivity (a factor *ca.* 44 less than for $n = 6$). Caution should be applied when interpreting barrier heights from DFT calculations and we have not performed an exhaustive study with different functionals. The answer may lie in the apparent need for greater fluxionality of the Pt_5^+ cluster during the reaction pathway than the prism/tetrahedral structures of Pt_6^+ and Pt_4^+ , respectively.

B. IR-MPD spectra

Fig. 4 shows the IR-MPD spectra recorded in depletion for $\text{Pt}_n(\text{N}_2\text{O})^+$ ($n = 1-8$) in the region $950-2400 \text{ cm}^{-1}$ covering the nitrous oxide N=N and N=O stretches. In Fig. 4 these bands in the free N_2O molecules are indicated with dashed lines at around 2224 cm^{-1} (N=N stretch) and 1285 cm^{-1} (N=O stretch), respectively. As discussed above, negligible $\text{Pt}_6(\text{N}_2\text{O})^+$ is produced and hence no spectrum could be recorded of this species.

The spectra of each species $n \geq 3$ exhibit clear features slightly blue-shifted from the free N_2O band positions. The presence of these bands, close to those of free nitrous oxide, clearly indicates molecularly-bound N_2O on the metal cluster.

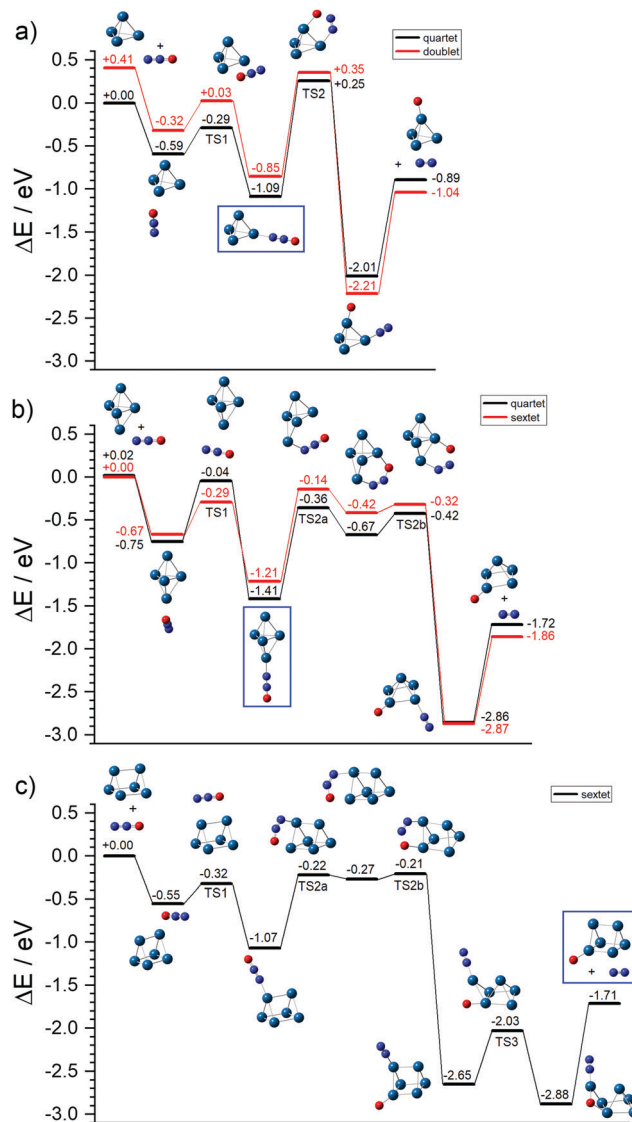


Fig. 3 Intrinsic reaction coordinate for (a) Pt_4^+ , (b) Pt_5^+ and (c) Pt_6^+ + N_2O entrance channels. Blue boxes highlight the predominant species observed in the mass spectrum for each n . The barrier to N_2O dissociation on Pt_n^+ cluster is pronounced for $n = 4$ and submerged for $n = 6$. This is reflected in the observed reactivity (see Fig. 2); Pt_4^+ is the least reactive favouring N_2O adsorption whereas Pt_6^+ does not form any adsorption products and mainly produces oxides. Only the lowest electronic states are shown. For $n = 4$, geometries of both doublet and quartet are virtually indistinguishable; for $n = 5$, they are not – higher in energy sextet structures are given in the ESI.†

The blue-shift of both bands indicates preferential N-binding on $n \geq 3$ clusters (supported by computational results below) and reflects the dominance of σ -donation from the nitrous oxide to the cationic Pt_n^+ cluster over π -back bonding. For the smallest species, $n = 1-2$, the observed vibrational bands are considerably broader and there is evidence of components both blue- and red-shifted with respect to the free N_2O stretches. Red-shifted bands, especially around the N=O stretch, are strong evidence for the presence of O-bound clusters, which have been seen before in similar, higher-resolution infrared



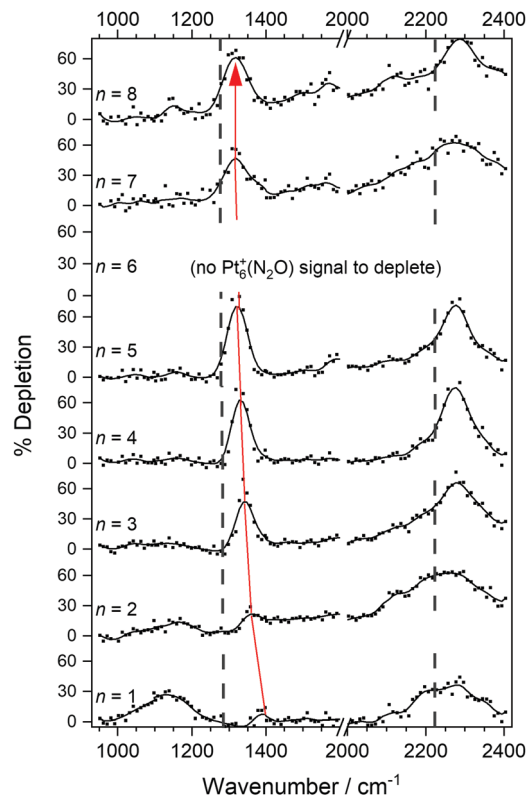


Fig. 4 IR-MPD spectra of $\text{Pt}_n(\text{N}_2\text{O})^+$ ($n = 1-8$) clusters recorded in depletion of the parent cluster ion. The dashed lines at 1285 cm^{-1} and 2224 cm^{-1} indicate the wavenumbers of the $\text{N}=\text{O}$ and $\text{N}=\text{N}$ stretches of free N_2O , respectively.⁵⁰

studies of $\text{M}^+(\text{N}_2\text{O})_n$ ($\text{M} = \text{Co}, \text{Rh}, \text{Ir}, \text{Cu}, \text{Ag}, \text{Au}, \text{Li}$ and Al).²⁹⁻³¹ The smallest clusters, with fewer degrees of freedom, are less efficiently annealed into lower energy (N-bound) structures, allowing the trapping of energetically higher-lying isomers, including O-bound structures.

The $\text{Pt}_8(\text{N}_2\text{O})^+$ cluster is intriguing amongst the larger clusters studied in that its spectrum exhibits both blue- and red-shifted bands in both spectral regions, possibly reflecting a mix of N- and O-bound structures. The O-bound structure has an $\text{N}=\text{O}$ stretch band, which is red-shifted by $>100 \text{ cm}^{-1}$, compared with the corresponding free N_2O band, indicating marked molecular activation.

A clear trend is observed in the frequency of the N-bound $\text{N}=\text{O}$ stretching band with cluster size. This band moves smoothly from $1390 \pm 5 \text{ cm}^{-1}$ on $n=1$ to $1315 \pm 5 \text{ cm}^{-1}$ by $n=8$ (shown in Fig. 4 with a red arrow). The same trend is observed in the calculated band positions which move from 1421 cm^{-1} for $\text{Pt}(\text{N}_2\text{O})^+$ to 1287 cm^{-1} for $\text{Pt}_5(\text{N}_2\text{O})^+$. The broader nature of the band in the $\text{N}=\text{N}$ stretch region makes it harder to discern any such trend in this region.

Fig. 5 compares the experimental spectra of $\text{Pt}_3(\text{N}_2\text{O})^+$ and $\text{Pt}_4(\text{N}_2\text{O})^+$ with those predicted for energetically low-lying calculated structures. The lowest energy calculated structures are inserted (*i.e.*, dissociative N_2O adsorption), but given the low binding energy of N_2 and the overall exothermicity of the dissociation, it is unlikely that such $\text{Pt}_n\text{O}(\text{N}_2)^+$ structures would

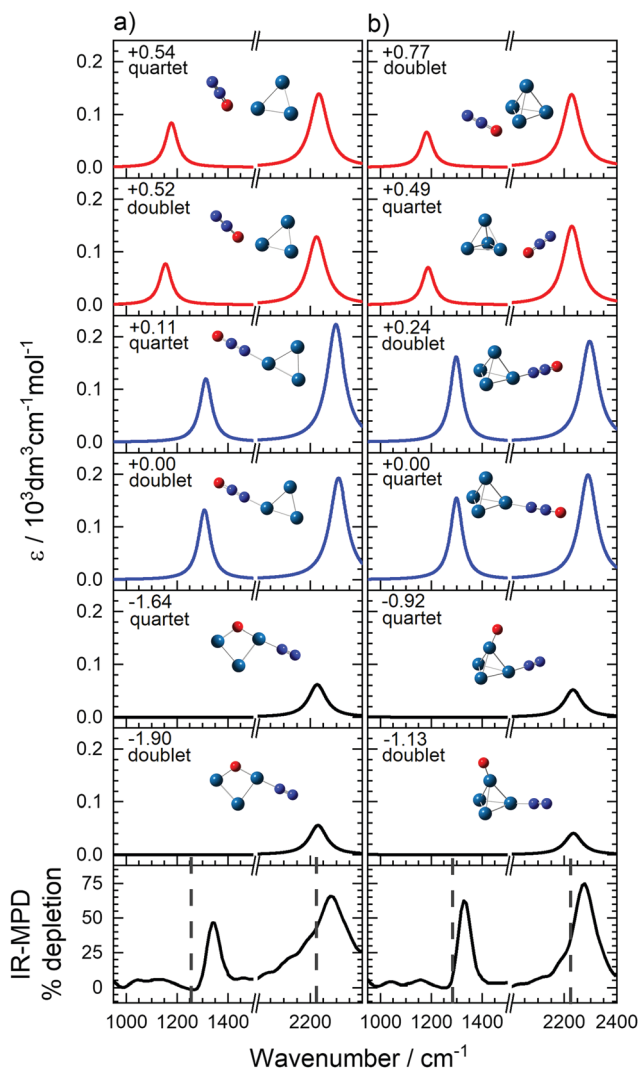


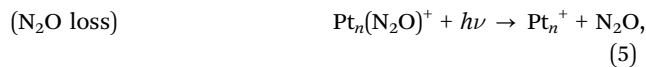
Fig. 5 Comparison of experimental and simulated IR-MPD spectra for a range of low-lying isomers of (a) $\text{Pt}_3(\text{N}_2\text{O})^+$ and (b) $\text{Pt}_4(\text{N}_2\text{O})^+$ complexes. All molecularly-bound isomers within 1 eV of the lowest energy structure are presented. Blue spectra represent N-bound isomers and red spectra – O-bound variants. The dashed lines at 1285 cm^{-1} and 2224 cm^{-1} represent the fundamental bands in free N_2O .⁵⁰

remain bound. The IR-MPD spectra clearly indicate the presence of molecularly-bound structures suggesting a kinetic barrier to dissociation. For this reason we choose the lowest-energy molecularly-bound structure as our zero of energy. Low-lying doublet and quartet electronic states are found for both clusters but the N-bound isomers lie lower in energy than corresponding O-bound isomers by approximately 0.5 eV in each case, supporting the assignments of the IR-MPD spectra made above. All structures are bound at single atom rather than bridging sites and the agreement between the simulated spectra and those observed experimentally is so good that there is no need to invoke the presence of any other structures in the beam.

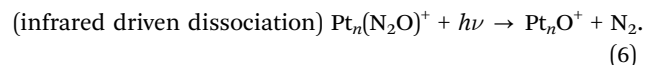
In any infrared action spectrum the depletion of a parent ion signal must be matched by an enhancement in the signal for some daughter species. By tracking parent ion depletions and absolute signal enhancements in different daughter channels



simultaneously, it is possible to determine the branching ratios for the two most likely possibilities:



and



Such an analysis is shown in Fig. 6 for $\text{Pt}_n(\text{N}_2\text{O})^+$ ($n = 3-5, 7, 8$) in the region of the N=O stretching mode (with very similar behaviour observed in the N=N stretch). A quantitative comparison of product channel enhancements *versus* parent ion depletion is a real challenge due to multiple species with similar spectra yielding the same fragmentation products. This affects net lineshapes and relative enhancements/depletion signal size in each channel. Nevertheless some clear pictures do emerge. In terms of reactivity, the smaller cluster sizes, $n = 3-5$ behave qualitatively differently to the $n = 7, 8$ clusters. For $\text{Pt}_n(\text{N}_2\text{O})^+$ ($n = 3-5$), excitation of the N=O stretch leads almost exclusively to N_2O loss (process (5)), consistent with the idea that, from the entrance-channel minimum, the $\text{Pt}_n^+ + \text{N}_2\text{O}$ dissociation threshold is reached before the transition state leading to nitrous oxide decomposition. By contrast, for $\text{Pt}_n(\text{N}_2\text{O})^+$ ($n = 7, 8$), comparable enhancements in both the Pt_n^+ and Pt_nO^+ daughter channels (processes (5) and (6)) imply that the reactive transition state lies below or at a comparable energy to the dissociation threshold. These observations are in good agreement with the reactivity data extracted from the time-of-flight spectra even down to the small Pt_3O^+ production following excitation of $\text{Pt}_3(\text{N}_2\text{O})^+$.

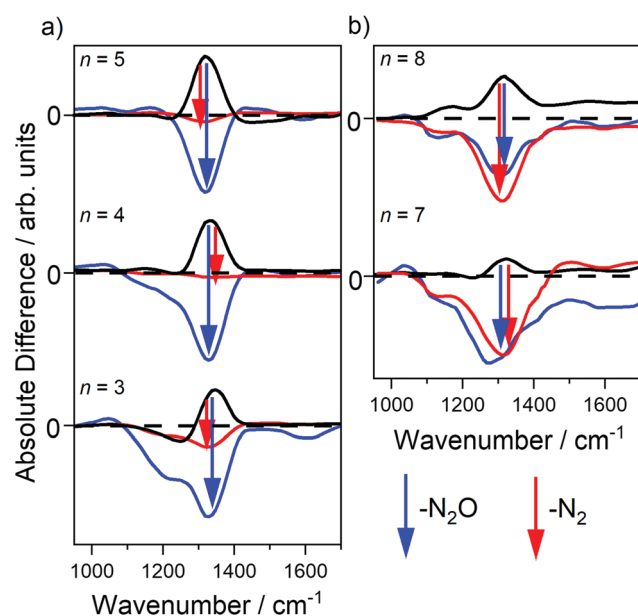


Fig. 6 (black) IR-MPD spectra of $\text{Pt}_n(\text{N}_2\text{O})^+$ clusters in the N_2O (N=O) stretch region. Red and blue spectra show the simultaneous enhancements observed in the Pt_nO^+ and Pt_n^+ mass channels representing IR driven reactive (N_2 loss) and desorptive (N_2O loss) processes.

Observation of efficient generation of the Pt_nO^+ daughter is a signal of infrared-induced chemistry on the surface of the cluster, a process which we have documented in several previous studies of other systems including $\text{Rh}_n(\text{N}_2\text{O})^+$,^{32,33} $\text{Rh}_n\text{O}(\text{N}_2\text{O})^+$,^{32,34} $\text{Pt}_n\text{O}_2(\text{CO})^+$,⁴⁵ and, recently, $\text{Au}_n(\text{OCS})^+$.⁵⁴ In several previous studies^{32,36} we have also demonstrated that the products observed following infrared excitation mirror those of collisional activation implying that we essentially “heat” the entrance-channel complexes until dissociation/reactive channels open. Previous studies have not revealed any mode-selective character to the chemistry induced and the current system is no exception. However, the ability to selectively increase the internal energy of a known cluster with spectral knowledge of its structure represents a unique feature in the exploration of these catalytically-relevant reactive potential energy surfaces.

V. Summary and conclusions

A combined experimental (IR-MPD) and computational study of nitrous oxide reacting with and binding to platinum cluster cations, Pt_n^+ ($n = 3-8$), has revealed key features on the potential energy surface of the $\text{Pt}_n^+ + \text{N}_2\text{O} \rightarrow \text{Pt}_n\text{O}^+ + \text{N}_2$ reaction. The laser ablation/molecular beam conditions employed in this study are shown, in most cases, to lead to the efficient formation of entrance-channel complexes on the reactive surface, the structures of which can be probed by multiple-photon dissociation action spectroscopy. One notable exception is the Pt_6^+ cluster, which reacts completely to generate the oxide with no evidence of $\text{Pt}_6(\text{N}_2\text{O})^+$ observed.

The observed reactivity can be well-understood in terms of potential energy surfaces calculated at the DFT level. Similarly, the simulated vibrational spectra for calculated low-energy entrance-channel complexes match well with the action spectra recorded. For several cluster sizes, clear evidence for infrared-driven cluster chemistry is observed in the loss of N_2 following infrared excitation of the N=O stretching mode of the parent $\text{Pt}_n(\text{N}_2\text{O})^+$. These results, too, are in quantitative agreement with calculated reactive barrier heights compared to N_2O binding energies.

Conflicts of interest

There are no conflicts to declare.

Acknowledgements

This work was funded in part by EPSRC under Programme Grant EP/L005913. The Oxford authors would like to acknowledge the use of the University of Oxford Advanced Research Computing (ARC) facility in carrying out this work: <https://doi.org/10.5281/zenodo.22558>. Financial support permitting research visits is also gratefully acknowledged from the Oxford-Berlin Research Partnership (Ref.: OXBER_STEM5, “A Collaborative Approach to Understanding Nitrogen Oxide Reduction at Metal Centres”). G. M. and A. E. G. thank Worcester and Magdalen Colleges, Oxford, respectively for their graduate studentships. A. F. thanks the Deutsche Forschungsgemeinschaft for his



Heisenberg Grant (FI893/5). Open Access funding provided by the Oxford University Agreement.

References

- 1 J. Pérez-Ramírez, F. Kapteijn, K. Schöffel and J. A. Moulijn, *Appl. Catal., B*, 2003, **44**, 117–151.
- 2 WMO (World Meteorological Organization), Scientific Assessment of Ozone Depletion: 2018, Global Ozone Research and Monitoring Project-Report No. 58, 588 pp., Geneva, Switzerland, 2018.
- 3 A. R. Ravishankara, J. S. Daniel and R. W. Portmann, *Science*, 2009, **326**, 123.
- 4 UNEP 2015, Synthesis of the 2014 Reports of the Scientific, Environmental Effects, and Technology & Economic Assessment Panels of the Montreal Protocol, United Nations Environment Programme (UNEP), Nairobi.
- 5 V. Rosca, M. Duca, M. T. de Groot and M. T. M. Koper, *Chem. Rev.*, 2009, **109**, 2209–2244.
- 6 G. Chinchin, P. Davies and R. J. Sampson, in *Catalysis: Science and Technology*, ed. J. R. Anderson and M. Boudart, Springer, Berlin, Heidelberg, 1987, vol. 8, pp. 1–67.
- 7 R. C. Stempel and S. W. Martens, *SAE Trans.*, 1974, **83**, 2358–2372.
- 8 A. Cho, *Science*, 2003, **299**, 1684–1685.
- 9 A. Ulvestad, A. Singer, J. N. Clark, H. M. Cho, J. W. Kim, R. Harder, J. Maser, Y. S. Meng and O. G. Shpyrko, *Science*, 2015, **348**, 1344–1347.
- 10 M. B. Knickelbein, *Annu. Rev. Phys. Chem.*, 1999, **50**, 79–115.
- 11 D. K. Böhme and H. Schwarz, *Angew. Chem., Int. Ed.*, 2005, **44**, 2336–2354.
- 12 D. J. Trevor, R. L. Whetten, D. M. Cox and A. Kaldor, *J. Am. Chem. Soc.*, 1985, **107**, 518–519.
- 13 D. J. Trevor, D. M. Cox and A. Kaldor, *J. Am. Chem. Soc.*, 1990, **112**, 3742–3749.
- 14 T. Hanmura, M. Ichihashi and T. Kondow, *J. Phys. Chem. A*, 2002, **106**, 11465–11469.
- 15 G. S. Jackson, F. M. White, C. L. Hammill, R. J. Clark and A. G. Marshall, *J. Am. Chem. Soc.*, 1997, **119**, 7567–7572.
- 16 C. Adlhart and E. Uggerud, *Chem. – Eur. J.*, 2007, **13**, 6883–6890.
- 17 C. Adlhart and E. Uggerud, *Chem. Commun.*, 2006, 2581–2582.
- 18 U. Achatz, C. Berg, S. Joos, B. S. Fox, M. K. Beyer, G. Niedner-Schatteburg and V. E. Bondybey, *Chem. Phys. Lett.*, 2000, **320**, 53–58.
- 19 M. Andersson and A. Rosén, *J. Chem. Phys.*, 2002, **117**, 7051–7054.
- 20 H. Yamamoto, K. Miyajima, T. Yasuike and F. Mafuné, *J. Phys. Chem. A*, 2013, **117**, 12175–12183.
- 21 K. Koszinowski, D. Schröder and H. Schwarz, *J. Phys. Chem. A*, 2003, **107**, 4999–5006.
- 22 I. Balteanu, O. Petru Balaj, M. K. Beyer and V. E. Bondybey, *Phys. Chem. Chem. Phys.*, 2004, **6**, 2910–2913.
- 23 P. A. Hintz and K. M. Ervin, *J. Chem. Phys.*, 1995, **103**, 7897–7906.
- 24 L. Lv, Y. Wang, Q. Wang and H. Liu, *J. Phys. Chem. C*, 2010, **114**, 17610–17620.
- 25 P. Ferrari, K. Hansen, P. Lievens and E. Janssens, *Phys. Chem. Chem. Phys.*, 2018, **20**, 29085–29090.
- 26 A. E. Green, J. Justen, W. Schöllkopf, A. S. Gentleman, A. Fielicke and S. R. Mackenzie, *Angew. Chem., Int. Ed.*, 2018, **57**, 14822–14826.
- 27 Y. Shi and K. M. Ervin, *J. Chem. Phys.*, 1998, **108**, 1757–1760.
- 28 O. P. Balaj, I. Balteanu, T. T. J. Roßteuscher, M. K. Beyer and V. E. Bondybey, *Angew. Chem., Int. Ed.*, 2004, **43**, 6519–6522.
- 29 E. M. Cunningham, A. S. Gentleman, P. W. Beardsmore, A. Iskra and S. R. Mackenzie, *J. Phys. Chem. A*, 2017, **121**, 7565–7571.
- 30 E. M. Cunningham, A. S. Gentleman, P. W. Beardsmore and S. R. Mackenzie, *Phys. Chem. Chem. Phys.*, 2019, **21**, 13959–13967.
- 31 E. M. Cunningham, A. S. Gentleman, P. W. Beardsmore and S. R. Mackenzie, *Mol. Phys.*, 2019, **117**, 2990–3000.
- 32 S. M. Hamilton, W. S. Hopkins, D. J. Harding, T. R. Walsh, M. Haertelt, C. Kerpel, P. Gruene, G. Meijer, A. Fielicke and S. R. Mackenzie, *J. Phys. Chem. A*, 2011, **115**, 2489–2497.
- 33 S. M. Hamilton, W. S. Hopkins, D. J. Harding, T. R. Walsh, P. Gruene, M. Haertelt, A. Fielicke, G. Meijer and S. R. Mackenzie, *J. Am. Chem. Soc.*, 2010, **132**, 1448–1449.
- 34 A. C. Hermes, S. M. Hamilton, W. S. Hopkins, D. J. Harding, C. Kerpel, G. Meijer, A. Fielicke and S. R. Mackenzie, *J. Phys. Chem. Lett.*, 2011, **2**, 3053–3057.
- 35 I. S. Parry, A. Kartouzian, S. M. Hamilton, O. P. Balaj, M. K. Beyer and S. R. Mackenzie, *Angew. Chem., Int. Ed.*, 2015, **54**, 1357–1360.
- 36 I. S. Parry, A. Kartouzian, S. M. Hamilton, O. P. Balaj, M. K. Beyer and S. R. Mackenzie, *J. Phys. Chem. A*, 2013, **117**, 8855–8863.
- 37 W. Schöllkopf, S. Gewinner, H. Junkes, A. Paarmann, G. von Helden, H. Bluem and A. M. Todd, *Proc. SPIE*, 2015, **9512**, 95121L.
- 38 A. Yanagimachi, K. Koyasu, D. Y. Valdivielso, S. Gewinner, W. Schöllkopf, A. Fielicke and T. Tsukuda, *J. Phys. Chem. C*, 2016, **120**, 14209–14215.
- 39 A. Fielicke, G. von Helden and G. Meijer, *Eur. Phys. J. D*, 2005, **34**, 83–88.
- 40 F. Weigend and R. Ahlrichs, *Phys. Chem. Chem. Phys.*, 2005, **7**, 3297–3305.
- 41 V. N. Staroverov, G. E. Scuseria, J. Tao and J. P. Perdew, *J. Chem. Phys.*, 2003, **119**, 12129–12137.
- 42 J. Tao, J. P. Perdew, V. N. Staroverov and G. E. Scuseria, *Phys. Rev. Lett.*, 2003, **91**, 146401.
- 43 M. J. Frisch, G. W. Trucks, H. B. Schlegel, G. E. Scuseria, M. A. Robb, J. R. Cheeseman, G. Scalmani, V. Barone, G. A. Petersson, H. Nakatsuji, X. Li, M. Caricato, A. V. Marenich, J. Bloino, B. G. Janesko, R. Gomperts, B. Mennucci, H. P. Hratchian, J. V. Ortiz, A. F. Izmaylov, J. L. Sonnenberg, D. Williams-Young, F. Ding, F. Lipparini, F. Egidi, J. Goings, B. Peng, A. Petrone, T. Henderson, D. Ranasinghe, V. G. Zakrzewski, J. Gao, N. Rega, G. Zheng, W. Liang, M. Hada, M. Ehara, K. Toyota, R. Fukuda, J. Hasegawa, M. Ishida, T. Nakajima, Y. Honda, O. Kitao, H. Nakai, T. Vreven, K. Throssell, J. A. Montgomery Jr., J. E. Peralta, F. Ogliaro, M. J. Bearpark, J. J. Heyd, E. N. Brothers, K. N. Kudin, V. N. Staroverov, T. A. Keith, R. Kobayashi, J. Normand,



- K. Raghavachari, A. P. Rendell, J. C. Burant, S. S. Iyengar, J. Tomasi, M. Cossi, J. M. Millam, M. Klene, C. Adamo, R. Cammi, J. W. Ochterski, R. L. Martin, K. Morokuma, O. Farkas, J. B. Foresman and D. J. Fox, *Gaussian 16 Revision C.01*, Gaussian, Inc., Wallingford CT, 2016.
- 44 K. P. Jensen, *J. Phys. Chem. A*, 2009, **113**, 10133–10141.
- 45 A. C. Hermes, S. M. Hamilton, G. A. Cooper, C. Kerpál, D. J. Harding, G. Meijer, A. Fielicke and S. R. Mackenzie, *Faraday Discuss.*, 2012, **157**, 213–225.
- 46 A. Fielicke, P. Gruene, M. Haertel, D. J. Harding and G. Meijer, *J. Phys. Chem. A*, 2010, **114**, 9755–9761.
- 47 D. J. Harding, C. Kerpál, D. M. Rayner and A. Fielicke, *J. Chem. Phys.*, 2012, **136**, 211103.
- 48 S. Grimme, S. Ehrlich and L. Goerigk, *J. Comput. Chem.*, 2011, **32**, 1456–1465.
- 49 D. Andrae, U. Häußermann, M. Dolg, H. Stoll and H. Preuß, *Theor. Chim. Acta*, 1990, **77**, 123–141.
- 50 G. Herzberg, *Molecular Spectra and Molecular Structure: II Infrared and Raman Spectra of Polyatomic Molecules*, Krieger, Malabar, Florida, 1991.
- 51 K. Fukui, *Acc. Chem. Res.*, 1981, **14**, 363–368.
- 52 H. P. Hratchian and H. B. Schlegel, *Theory and Applications of Computational Chemistry: The First 40 Years*, Elsevier, Amsterdam, 2005.
- 53 C. Kerpál, D. J. Harding, A. C. Hermes, G. Meijer, S. R. Mackenzie and A. Fielicke, *J. Phys. Chem. A*, 2013, **117**, 1233–1239.
- 54 A. E. Green, S. Schaller, G. Meizyte, B. J. Rhodes, S. P. Kealy, A. S. Gentleman, W. Schöllkopf, A. Fielicke and S. R. Mackenzie, *J. Phys. Chem. A*, 2020, **124**, 5389–5401.

